

Forecasting high-dimensional functional time series: Application to sub-national age-specific mortality

Cristian F. Jiménez-Varón  and Ying Sun  *

CEMSE Division

King Abdullah University of Science and Technology

Han Lin Shang 

Department of Actuarial Studies and Business Analytics

Macquarie University

February 14, 2024

Abstract

We study the modeling and forecasting of high-dimensional functional time series (HDFTS), which can be cross-sectionally correlated and temporally dependent. We introduce a decomposition of the HDFTS into two distinct components: a deterministic component and a residual component that varies over time. The decomposition is derived through the estimation of two-way functional analysis of variance. A functional time series forecasting method, based on functional principal component analysis, is implemented to produce forecasts for the residual component. By combining the forecasts of the residual component with the deterministic component, we obtain forecast curves for multiple populations. We apply the model to age- and sex-specific mortality rates in the United States, France, and Japan, in which there are 51 states, 95 departments, and 47 prefectures, respectively. The proposed method is capable of delivering more accurate point and interval forecasts in forecasting multi-population mortality than several benchmark methods considered.

Keywords: functional time series, forecasting, functional principal component analysis; functional ANOVA; functional median polish; sub-national mortality.

arXiv:2305.19749v2 [stat.ME] 13 Feb 2024

*Postal address: CEMSE Division, Statistics Program, King Abdullah University of Science and Technology, Thuwal 23955-6900, Saudi Arabia. E-mail: ying.sun@kaust.edu.sa

1 Introduction

In recent years, most countries worldwide have seen continuous drops in mortality rates, which are also associated with aging populations. For planning purposes, policymakers from insurance firms and government departments demand more precise mortality forecasts. Several statistical methods have been presented for forecasting age-specific central mortality rates, life-table death counts, or survival functions (see, e.g., [Booth, 2006](#); [Currie et al., 2004](#); [Booth and Tickle, 2008](#); [Shang et al., 2011](#); [Basellini et al., 2023](#)).

One of the most outstanding contributions in this field is that of [Lee and Carter \(1992\)](#), who use a principal component method to derive a single time-varying index of the level of mortality rates, from which forecasts are obtained using a random walk with drift. Subsequently, several approaches have modified and extended the Lee-Carter method. For instance, [Renshaw and Haberman \(2003\)](#) propose the age-period-cohort Lee Carter method; [Hyndman and Ullah \(2007\)](#) propose a functional data approach along with nonparametric smoothing and high-order principal components; [Giroi and King \(2008\)](#) and [Wiśniowski et al. \(2015\)](#) consider Bayesian techniques for the estimation and forecasting of the Lee-Carter model; and [Li et al. \(2013\)](#) extend the Lee-Carter method to approximate age pattern rotation for long-term projections.

One major drawback of the Lee-Carter method and previous contributions is that they mainly focus on forecasting mortality for a single population. Each population can be further categorized based on gender, state, ethnic group, socioeconomic status, and other factors. Individual forecasts, even when based on identical extrapolating processes, may, in the long run, imply increased divergence in mortality rates, contrary to the expected and observed trend toward global convergence (see, e.g., [Li, 2012](#); [Pampel, 2005](#); [Hyndman et al., 2013a](#)).

Joint modeling mortality for two or more populations simultaneously is critical; it considers data correlation and may discriminate between long-term and short-term impacts in mortality evolution. Finally, joint modeling incorporates additional information from other populations that can be used to enhance forecast accuracy. Various proposals have tackled the problem of combining several populations for forecasting. For instance, [Shang \(2016\)](#) proposes multivariate and multilevel functional data approaches for forecasting age-specific mortality rates for two or more populations in developed countries with high-quality vital registration systems. [Shang and Hyndman \(2017\)](#) and [Shang and Haberman \(2017\)](#) advocate employing a grouped functional time series methodology in conjunction with a bootstrap method to provide point and interval forecasts

of mortality rates that are correctly aggregated across different disaggregation parameters.

Functional analysis of variance (ANOVA) is a common option for joint modeling with functional data (Ramsay and Silverman, 2006, Chapter 13). Functional ANOVA models evaluate the functional impacts of categorical factors by determining how functions differ at different levels of these factors. Functional ANOVA models have proven usefulness in analyzing data in a wide range of applications, such as human tactile perception (Spitzner et al., 2003), menstrual cycle data (Brumback and Rice, 1998), and circadian rhythms with random effects and smoothing spline ANOVA decomposition (Wang et al., 2003). In particular, Kaufman and Sain (2010) establishes a Bayesian framework for functional ANOVA modeling to estimate the effect of geographic regions on Canadian temperatures.

Sun and Genton (2012) propose a functional median polish (FMP-ANOVA) modeling as an extension of the univariate median polish proposed by Tukey (1977) and Mosteller and Tukey (1977). FMP-ANOVA computes the functional grand effect and functional main factor effects in an additive model without factor interaction. It is a robust statistical technique for studying the effects of factors on response since it replaces the mean with the median (Emerson and Hoaglin, 1983). Sun and Genton (2012) present a functional rank test to determine the significance of functional main factor effects. Additionally, they prove the robustness of FMP-ANOVA by comparing its performance to the functional ANOVA model fitted by means (FM-ANOVA).

In the functional data analysis (FDA) approach (Ramsay and Silverman, 2006), it is assumed that the mortality rate in each year follows an underlying smooth function of age. When mortality rates are collected over time, we refer to the data as functional time series (FTS). Because of observational noise, observed mortality rates are not smooth across ages. We employ a penalized regression spline smoothing with monotonic constraint (Wood, 1994) to create smooth functions and deal with possible missing data. It considers the shape of the log mortality curve (see also Hyndman and Ullah, 2007; Shang and Hyndman, 2017). The smooth shape of age-specific mortality rates over age in each year is a distinguishing feature, which can improve short-term forecast accuracy (see, e.g., Basellini and Camarda, 2019; Yang et al., 2024).

Smoothing techniques can better capture the underlying trend of mortality changes, reducing the impact of missing values and measurement noise in various sub-national series (Yang et al., 2024). Functional ANOVA models provide an insightful decomposition of functional mortality rates into a deterministic component (such as populations or states as in the functional factor

effects) and a functional residual component that varies over time. The functional residuals are inputs for mortality forecasting.

Hence, functional time series forecasting methods often require efficient data reduction algorithms, since functional residuals are infinite-dimensional functions. For example, the most often used approach for this purpose is functional principal component analysis (FPCA). FPCA represents functional data on their eigenfunction basis. Several studies discuss FPCA, in particular, [Hall and Hosseini-Nasab \(2006\)](#) and [Hall et al. \(2006\)](#) for theoretical properties, [Viviani et al. \(2005\)](#) and [Locantore et al. \(1999\)](#) for empirical applications, [Shang \(2014\)](#) and [Wang et al. \(2016\)](#) for surveys.

In the FTS literature, different approaches are presented regarding the construction of prediction intervals. For instance, [Antoniadis et al. \(2006, 2016\)](#) execute one-step-ahead prediction using a nonparametric wavelet kernel; pointwise prediction intervals are produced using a re-sampling approach. Some other contributions, such as [Raña et al. \(2016\)](#) and [Vilar et al. \(2018\)](#), use model-based bootstrap procedures for constructing pointwise prediction intervals for one-step-ahead prediction. Such approaches are mainly based on assumptions on the data-generating process under the functional autoregressive model of order 1 (FAR(1)).

[Aue et al. \(2015\)](#) introduces an approach for constructing prediction intervals, in which a tuning parameter is selected to achieve the smallest distance between the empirical and nominal coverage probabilities based on the in-sample data. [Paparoditis \(2018\)](#) presents a sieve bootstrap approach for FTS that employs the vector autoregressive (VAR) representation of the time series of Fourier coefficients appearing in the Karhunen-Loève expansion of the functional process. For a stationary series, the VAR representation can be written forward and backward. [Paparoditis and Shang \(2023\)](#) introduce a sieve-bootstrap approach for constructing prediction bands for FTS that considers the different sources of error, including the model misspecification error, affecting the conditional distribution of the estimated functional residuals.

In the context of high-dimensional functional time series (HDFTS), [Zhou and Dette \(2023\)](#) derived Gaussian and multiplier bootstrap approximations for sums of HDFTS. By utilizing these approximations, they were able to construct joint simultaneous confidence bands for the mean functions and develop a hypothesis test to assess whether the mean functions in the panel dimension exhibit parallel behavior. [Hallin et al. \(2023\)](#) investigated the representation of HDFTS using a factor model, identifying conditions on the eigenvalues of the covariance operator crucial

for establishing the existence and uniqueness of the factor model. [Gao et al. \(2019\)](#) adopted a two-stage approach combining truncated principal component analysis and a separate scalar factor model for the resulting panels of scores, while [Tavakoli et al. \(2023\)](#) introduced a functional factor model with a functional factor loading and a vector of real-valued factors, and [Guo et al. \(2022\)](#) considered a functional factor model with a real-valued factor loading and a functional factor. Additionally, [Tang et al. \(2022\)](#) studied clustering problems for age-specific mortality rates, an example of HDFTS, and [Li et al. \(2023\)](#) proposed hypothesis tests for change point detection, change point estimation, and clustering of change points in HDFTS using an information criterion.

In the realm of estimating HDFTS models, [Guo and Qiao \(2023\)](#) introduced a three-step procedure that incorporates a novel functional stability measure, the non-asymptotic properties of functional principal component analysis (FPCA), and a regularization approach for estimating autoregressive coefficients. Moreover, [Tan et al. \(2024\)](#) proposed dynamic weak separability as a characterization of the two-way dependence structure in multivariate functional time series, developing a unified framework for functional graphical models and dynamic principal component analysis. Finally, [Chang et al. \(2023\)](#) presented a three-step framework for statistical learning of HDFTS with errors, incorporating autocovariance-based dimension reduction and a novel block regularized minimum distance estimation.

In this paper, we propose an innovative forecasting approach for HDFTS. Our method begins with the estimation of a two-way functional ANOVA model, that decomposes the HDFTS into a deterministic component and functional residuals that vary over time. Such estimation of the functional ANOVA model can be carried out by either means or medians. In particular, in the presence of functional outliers, FMP-ANOVA has been proven to be robust against such outliers ([Sun and Genton, 2012](#)). After removing the deterministic component, a functional principal component regression is deployed to model and forecast the functional residual component. Finally, we obtain forecast curves for several populations by combining the forecasts of the functional residuals that vary over time with the deterministic components. The proposed FTS forecasting method based on a decomposition from the estimation of a two-way analysis of variance model is compared with existing methods such as the factor models from [Gao et al. \(2019\)](#) and [Tavakoli et al. \(2023\)](#).

We investigate the proposed method's point and interval forecast accuracies using age- and sex-specific mortality rates from the US, France, and Japan. For the US, we consider 51 states from

1959 to 2020; for France, 95 departments from 1968 to 2021; and for Japan, 47 prefectures from 1975 to 2020. We consider the mean relative absolute prediction error (MAPE) and root mean relative squared prediction error (RMSPE) for evaluating point forecast accuracy. For comparing interval forecast accuracy, we study the difference between the empirical and nominal coverage probabilities and the mean interval score of [Gneiting and Raftery \(2007\)](#) and [Gneiting and Katzfuss \(2014\)](#).

The remainder of this paper is structured as follows. In § 2, we present the US, French, and Japanese sub-national mortality rates. In § 3, we introduce a FTS forecasting method for producing point and interval forecasts. The proposed FTS forecasting method is based on both functional ANOVA decomposition and FPCA. We evaluate and compare point and interval forecast accuracies with existing joint time series forecasting methods in § 4.1 and § 4.2, respectively. § 5 concludes and offers some ideas on how the methodology presented can be extended.

2 Age-specific mortality rates in the United States, France, and Japan

The United States Mortality Database documents a historical set of complete state-level life tables designed to foster research on geographic variations in mortality across the US and to monitor trends in health inequalities ([United States Mortality Database, 2023](#)). This data set currently includes complete and abridged life tables by sex for each of the nine US Census Divisions, four Census Regions, 50 States, and the District of Columbia, for each year between 1959 and 2020, with mortality up to age 110. To motivate the discussion, consider the first row of Figure 1 showing annual age- and sex-specific \log_{10} mortality rates for the US.

The French Human Mortality Database ([Bonnet, 2020](#)) allows the general public to assess mortality data by region. We are interested in the dynamic changes in the mortality rates in France at the departmental level and, particularly, in the age-specific mortality rates in a single-year interval by sex. In Europe, France has 95 departments, with mortality data up to age 110. We examine age groupings ranging from 0 to 100 in single years of age, with the last age group including all ages above 100. These departments are Seine and Seine et Oise, which have been removed from our further analyses. We examine age groupings ranging from 0 to 100 in single years of age, with the last age group including ages above 100. The annual age-specific \log_{10}

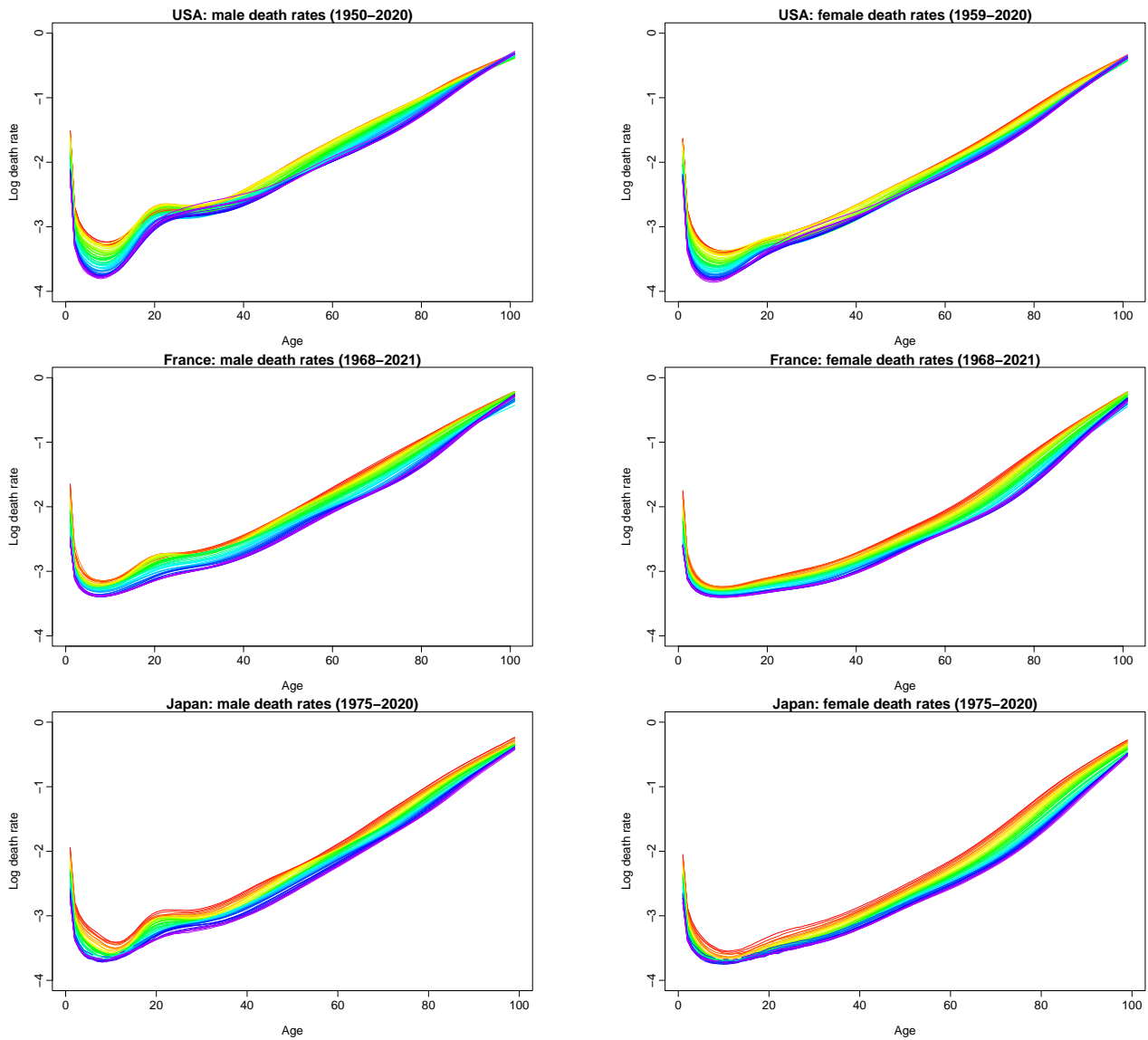


Figure 1: The smoothed age-specific \log_{10} mortality rates between 1959 and 2020 in the US, between 1968 and 2021 in France, and between 1975 and 2020 in Japan. Curves are ordered chronologically using the rainbow color palette, the oldest curves are shown in red, with the most recent curves in violet.

mortality rates for the French females and males between 1968 and 2021 are shown in the second row of Figure 1.

We investigate the Japanese age-specific mortality rates from 1975 to 2020, as obtained from the [Japanese Mortality Database \(2023\)](#). The mortality rates are the ratios of death counts to population exposure in the relevant year for the given age (based on a one-year age group). We examine age groupings ranging from 0 to 98 in single years of age, with the last age group including all ages at and above 99. We do not have the same truncation age as for the previous cases due to missing values in some of the prefectures for older ages. The annual age-specific \log_{10} mortality rates for Japanese females and males between 1975 and 2020 are shown in the last row of Figure 1. Due to ease of interpretability, we refer by log to the base 10 logarithm (\log_{10}).

3 Methodology

We introduce two decompositions based on functional analysis of variance in § 3.1, the functional median polish (FMP-ANOVA) approach of [Sun and Genton \(2012\)](#), and the functional mean analysis of variance (FM-ANOVA). § 3.2 reports the forecasting method for FTS based on FPCA. § 3.3 describes the proposed FTS forecasting method based on the estimation of a functional analysis of variance decomposition and FPCA. § 3.4 explains a sieve bootstrap methodology to obtain prediction intervals for mortality curves. For consistency, we refer to departments and prefectures as states.

3.1 A two-way functional ANOVA decomposition

Let $\mathcal{Y}_{t,s}^g(u)$ be the \log_{10} mortality rate for age u , state s , gender g at year t . By treating age u as a continuum, a two-way functional ANOVA model can be estimated for FTS. In this way, $\mathcal{Y}_{t,s}^g(u)$ can be decomposed as:

$$\mathcal{Y}_{t,s}^g(u) = \mu(u) + \alpha_s(u) + \beta^g(u) + \mathcal{X}_{t,s}^g(u), \quad (1)$$

where, $\mu(u)$ denotes the functional grand effect, $\alpha_s(u)$ denotes the functional row effect and, $\beta^g(u)$ denotes the functional column effect. Although u ($u \in \mathcal{I} \subset \mathbb{R}$) is a continuous variable, it can only be observed at a set of grid points, such as (u_1, \dots, u_p) . For each state s and gender g , we considered replicates the years t with time horizon, for $t = 1, \dots, T$, $s = 1, \dots, n_s$, and

$g = \text{Female}(F), \text{Male}(M)$. Finally, $\mathcal{X}_s^g(u) = [\mathcal{X}_{1,s}^g(u), \dots, \mathcal{X}_{T,s}^g(u)]$ denotes the functional residual process for the state s and gender g . The model described in (1), can be estimated by two approaches: The FM-ANOVA model and the FMP-ANOVA approach of Sun and Genton (2012). In particular, if the model in (1), is estimated through the FMP-ANOVA decomposition, it satisfies that $\forall u \in \mathcal{I}, \text{median}_s\{\alpha_s(u)\} = 0, \text{median}_g\{\beta^g(u)\} = 0, \text{median}_s\{\mathcal{X}_{t,s}^g(u)\} = \text{median}_g\{\mathcal{X}_{t,s}^g(u)\} = 0$ for all t (Sun and Genton, 2012).

Alternatively, the functional ANOVA model in (1) can be fitted by means (FM-ANOVA) with (Ramsay and Silverman, 2006; Sun and Genton, 2012)

$$\begin{aligned}\widehat{\mu}(u) &= \frac{1}{T} \sum_{s=1}^{n_s} \sum_{g=1}^{n_g} \sum_{t=1}^T \mathcal{Y}_{t,s}^g(u) \\ \widehat{\alpha}_s(u) &= \frac{1}{T} \sum_{g=1}^{n_g} \sum_{t=1}^T \mathcal{Y}_{t,s}^g(u) - \widehat{\mu}(u) \\ \widehat{\beta}^g(u) &= \frac{1}{T} \sum_{s=1}^{n_s} \sum_{t=1}^T \mathcal{Y}_{t,s}^g(u) - \widehat{\mu}(u).\end{aligned}$$

In the FM-ANOVA decomposition, there exist some identifiability constraints, so that for all $u \in \mathcal{I}, \sum_{s=1}^{n_s} \alpha_s(u) = \sum_{g=1}^{n_g} \beta^g(u) = 0$, and $\sum_{s=1}^{n_s} \mathcal{X}_{t,s}^g(u) = \sum_{g=1}^{n_g} \mathcal{X}_{t,s}^g(u) = 0$ for all t (Ramsay and Silverman, 2006, Chapter 13).

3.2 Functional time series forecasting method

We introduce the FTS forecasting approach based on the FPCA which relies on an accurate estimate of the covariance function. A brief description of the estimation of the covariance function is given in § 3.2.1. § 3.2.2 presents the basic ideas on FPCA designed for FTS forecasting.

3.2.1 Covariance function

For a given state s and gender g , denote $\mathcal{X}_{t,s}^g(u)$ a stochastic process defined on a compact set \mathcal{I} , with finite variance $\int_{\mathcal{I}} \mathbb{E} \left((\mathcal{X}_{t,s}^g(u))^2 \right) < \infty$. Furthermore, $\mathcal{X}_{t,s}^g(u)$ can be seen as a stationary ergodic FTS exhibiting stationarity and ergodicity. In essence, the statistical features of a stochastic process will not vary over time, and they can be obtained from a single, sufficiently long sample of the process. The covariance function of $\mathcal{X}_{t,s}^g(u)$ is defined to be the function $C(u, v) : \mathcal{I} \times \mathcal{I} \rightarrow \mathbb{R}$, such that

$$\begin{aligned}C(u, v) &= \text{Cov} \left(\mathcal{X}_{t,s}^g(u), \mathcal{X}_{t,s}^g(v) \right) \\ &= \mathbb{E} \left[\mathcal{X}_{t,s}^g(u) \mathcal{X}_{t,s}^g(v) \right].\end{aligned}\tag{2}$$

By assuming $\mathcal{X}_{t,s}^g(u)$ is a continuous and square-integrable function, the function $C(u, v)$ induces the kernel operator $L^2(\mathcal{I}) \rightarrow L^2(\mathcal{I}), \phi \rightarrow C\phi$, given by

$$(C\phi)(u) = \int_{\mathcal{I}} C(u, v)\phi(v)dv.$$

3.2.2 Functional principal component analysis

With the covariance function defined in (2), and via Mercer's lemma (Mercer and Forsyth, 1909), there exists an orthonormal sequence (ϕ_k) of continuous function in $L^2(\mathcal{I})$ and a non-increasing sequence of positive numbers θ_k , such that

$$C(u, v) = \sum_{k=1}^{\infty} \theta_k \phi_k^g(u) \phi_k^g(v),$$

where, the orthonormal functions $[\phi_1^g(u), \phi_2^g(u), \dots]$ are referred as the functional principal components. We can project the FTS $\mathcal{X}_{t,s}^g(u)$ onto a collection of orthogonal functional principal components ϕ_k^g via the inner product in the corresponding Hilbert space. This leads to the Karhunen-Loève expansion of the realization of the stochastic process $\mathcal{X}_{t,s}^g(u)$ that can be expressed as,

$$\mathcal{X}_{t,s}^g(u) = \bar{\mathcal{X}}_s^g(u) + \sum_{k=1}^{\infty} \Gamma_{k,t,s}^g \phi_{k,s}^g(u),$$

where $\Gamma_{k,t,s}^g = \langle \mathcal{X}_{t,s}^g(u) - \bar{\mathcal{X}}_s^g(u), \phi_{k,s}^g(u) \rangle$, denotes the k^{th} set of principal component scores for time t .

3.3 Point forecasts based on a two-way functional ANOVA decomposition

Define $\mathcal{Y}_{t,s}^g(u), t = 1, 2, \dots, T$ as a set of smoothed sub-national mortality rates functions, with T representing the number of total smoothed curves. For instance, assume that each $\mathcal{Y}_{t,s}^g(u)$ is a square-integrable function defined at the same interval of age. Through a two-way functional ANOVA decomposition approach, as described in § 3.1, $\mathcal{Y}_{t,s}^g(u)$ can be decomposed into two main components: (1) a deterministic component; and (2) a residual component that varies over time. The estimated deterministic component includes the functional grand effect $\hat{\mu}(u)$, functional row effect $\hat{\alpha}_s(u)$, and functional column effect $\hat{\beta}^g(u)$. The estimated component that varies over time refers to the functional residuals $\hat{\mathcal{X}}_s^g(u) = [\hat{\mathcal{X}}_{1,s}^g, \dots, \hat{\mathcal{X}}_{T,s}^g]$. That is

$$\underbrace{\hat{\mathcal{X}}_{t,s}^g(u)}_{\text{Residual}} = \mathcal{Y}_{t,s}^g(u) - \underbrace{[\hat{\mu}(u) + \hat{\alpha}_s(u) + \hat{\beta}^g(u)]}_{\text{deterministic}}.$$

When estimating the two-way functional ANOVA model in equation (1) using either the FM-ANOVA or FMP-ANOVA approaches, it is important to note that these decompositions separate the functional time series (FTS) into a deterministic component and a residual component. However, regardless of the chosen estimation method, these decompositions ensure the exact reconstruction of the original data.

Once the deterministic components are removed from the decomposition of $\mathcal{Y}_{t,s}^g(u)$, the residual components are used for FPCA as described in § 3.2. To incorporate the correlation between the residual components, $\widehat{\mathcal{X}}_s^g(u)$ can be stacked as for a given state s for female and male populations [Let $\widehat{\mathcal{X}}_s(u) = [\widehat{\mathcal{X}}_s^F(u), \widehat{\mathcal{X}}_s^M(u)]^\top$]. Let $\widehat{C}(u, v)$ be an estimator of the covariance function defined in (3.2.1) for the estimated residuals $\widehat{\mathcal{X}}_{t,s}(u) = [\widehat{\mathcal{X}}_{t,s}^F(u), \widehat{\mathcal{X}}_{t,s}^M(u)]^\top$. via Mercer's lemma $\widehat{C}(u, v)$ can be approximated by,

$$\widehat{C}(u, v) = \sum_{k=1}^T \widehat{\theta}_k \widehat{\phi}_k(u) \widehat{\phi}_k(v).$$

Through functional principal component analysis, it can be decomposed as follows:

$$\begin{aligned} \widehat{\mathcal{X}}_{t,s}(u) &= \overline{\widehat{\mathcal{X}}}_s(u) + \sum_{k=1}^{\infty} \widehat{\Gamma}_{k,t,s} \widehat{\phi}_{k,s}(u) \\ &= \overline{\widehat{\mathcal{X}}}_s(u) + \sum_{k=1}^K \widehat{\Gamma}_{k,t,s} \widehat{\phi}_{k,s}(u) + \widehat{\varepsilon}_{t,s}(u), \end{aligned}$$

where $[\widehat{\phi}_{1,s}(u), \dots, \widehat{\phi}_{K,s}(u)]$ is a set of orthogonal basis functions commonly known as a functional principal component for the s^{th} state, with $\widehat{\Gamma}_{k,t,s}$ as their related principal component scores for $k = 1, \dots, K, t = 1, \dots, T$; and $\widehat{\varepsilon}_{t,s}(u)$ denotes the model truncation error function with mean zero and finite variance. We select K by the eigenvalue ratio (EVR) criterion of (Li et al., 2021), such estimator is obtained simply by minimizing the ratio of two adjacent eigenvalues arranged in descending order.

$$K = \underset{k:1 \leq k \leq k_{\max}}{\operatorname{argmin}} \left\{ \frac{\lambda_{k+1}}{\lambda_k} \times \mathbb{1}\{\lambda_k > \tau\} + \mathbb{1}\{\lambda_k < \tau\} \right\},$$

where, $\mathbb{1}\{\cdot\}$ represents the binary indicator function. Customary, $\tau = 0.001$ and k_{\max} can be set as T . The selection of K is a crucial step, as the accuracy of the forecasting method relies heavily on choosing the appropriate number of principal components. It is important to note that Lam and Yao (2012) (Theorem 2) has demonstrated that the selected value of K is consistent and optimal.

There are different alternatives for determining the number of retained components: (1) scree plots or the fraction of variance explained by the first few functional principal components (Chiou,

2012); (2) pseudo-versions of Akaike information criterion and Bayesian information criterion (Yao et al., 2005); (3) predictive cross validation leaving out one or more curves (Ramsay and Silverman, 2006); (4) bootstrap methods (Hall and Vial, 2006); (5) eigenvalue ratio criterion (Ahn and Horenstein, 2013).

Collectively modeling multiple populations requires truncating the K^{th} functional principal components of all time series

$$\widehat{\mathcal{X}}_{t,s}(u) \approx \widehat{\Phi}_s(u) \widehat{\Gamma}_{t,s},$$

where $\widehat{\mathcal{X}}_{t,s}(u) = [\widehat{\mathcal{X}}_{t,s}^{\text{F}}(u), \widehat{\mathcal{X}}_{t,s}^{\text{M}}(u)]^{\top}$, and

$$\widehat{\Gamma}_{t,s} = \left[\widehat{\Gamma}_{1,t,s}^{\text{F}}, \dots, \widehat{\Gamma}_{K,t,s}^{\text{F}}, \widehat{\Gamma}_{1,t,s}^{\text{M}}, \dots, \widehat{\Gamma}_{K,t,s}^{\text{M}} \right]^{\top},$$

is a $((2 \times K) \times 1)$ vector of principal component scores. $\widehat{\Phi}_s(u)$ is a $2 \times (2 \times K)$ matrix that contains the associated basis functions, in which $\widehat{\Phi}_s(u)$ is given by

$$\widehat{\Phi}_s(u) = \begin{pmatrix} \widehat{\phi}_{1,1}^{\text{F}}(u) & \dots & \widehat{\phi}_{K,1}^{\text{F}}(u) & \dots & \dots \\ \dots & \dots & \widehat{\phi}_{1,2}^{\text{M}}(u) & \dots & \widehat{\phi}_{K,2}^{\text{M}}(u) \end{pmatrix}.$$

By conditioning on $\widehat{\Phi}_s(u)$, we can now obtain the h -step-ahead point forecasts as follows

$$\begin{aligned} \widehat{\mathcal{X}}_{T+h|T,s}(u) &= \mathbb{E} \left[\widehat{\mathcal{X}}_{T+h,s}(u) \mid \widehat{\mathcal{X}}_{1,s}(u), \dots, \widehat{\mathcal{X}}_{T,s}(u); \widehat{\Phi}_s(u) \right] \\ &= \overline{\widehat{\mathcal{X}}}_s(u) + \widehat{\Phi}_s(u) \widehat{\Gamma}_{T+h|T,s}, \end{aligned}$$

where the empirical mean function $\overline{\widehat{\mathcal{X}}}_s(u) = [\overline{\widehat{\mathcal{X}}}_s^{\text{F}}(u), \overline{\widehat{\mathcal{X}}}_s^{\text{M}}(u)]$. In this paper, we use the univariate time series forecasting method of Hyndman and Shang (2009) to obtain the forecast principal component score $\widehat{\Gamma}_{T+h|T,s}$ (see also Shang and Hyndman, 2017; Shang and Yang, 2021). Alternative to a univariate time series method, a multivariate time series forecasting method, such as VAR, can also be implemented in this step. In Appendix A.1, we compare the univariate and multivariate time series forecasting approaches for the three datasets presented in § 4.1 when computing point forecast.

Once the forecasted functional residuals are obtained, we add back the deterministic component from the functional ANOVA decomposition used. As this does not vary over time, the overall h -step-ahead point forecast is defined as

$$\widehat{\mathcal{Y}}_{T+h|T,s}^g(u) = \widehat{\mu}(u) + \widehat{\alpha}_s(u) + \widehat{\beta}^g(u) + \widehat{\mathcal{X}}_{T+h|T,s}^g(u).$$

3.4 Construction of prediction intervals

In the functional-ANOVA decompositions described in § 3.1, we consider joint modeling for both female and male populations to obtain the functional residuals. In this section, we use the functional residuals for each population separately to compute prediction intervals for quantifying forecast uncertainty using the approaches proposed by Paparoditis and Shang (2023) and Aue et al. (2015). The final prediction intervals are generated after adding back the deterministic components removed from the functional ANOVA decomposition. The procedure can be described as follows.

- 1) Center the observed functional time series by calculating $\mathcal{Z}_{t,s}^g(u) = \hat{\mathcal{X}}_{t,s}^g(u) - \bar{\mathcal{X}}_s^g(u)$, where $\bar{\mathcal{X}}_s^g(u) = \frac{1}{T} \sum_{t=1}^T \hat{\mathcal{X}}_{t,s}^g(u)$.
- 2) Apply the FPCA decomposition to $\mathcal{Z}_s^g(u) = [\mathcal{Z}_{1,s}^g(u), \dots, \mathcal{Z}_{T,s}^g(u)]$ to obtain a set of estimated functional principal components and their associated scores.
- 3) Fit a vector autoregression of order p , VAR(p), process to the “forward” series of the estimated scores; that is,

$$\hat{\Gamma}_{m,s}^g = \sum_{j=1}^p A_{j,p} \hat{\Gamma}_{m-j,s}^g + \epsilon_{m,s}^g, \quad m = p+1, \dots, T,$$

with $\epsilon_{m,s}^g$ being the residuals and $A_{j,p}$ denotes the forward VAR(p) coefficient. Generate

$$\hat{\Gamma}_{T+h,s}^{g,*} = \sum_{j=1}^p A_{j,p} \hat{\Gamma}_{T+h-j,s}^{g,*} + \epsilon_{T+h,s}^{g,*}$$

where we set $\hat{\Gamma}_{T+h-j}^{g,*} = \hat{\Gamma}_{T+h-j}$ if $T+h-j \leq T$ and $\epsilon_{T+h,s}^{g,*}$ is independent and identically distributed (iid) resampled from the set of centered residuals $(\epsilon_{m,s}^g - \bar{\epsilon}_s^g)$, $\bar{\epsilon}_s^g = (T-p)^{-1} \sum_{m=p+1}^T \epsilon_{m,s}^g$. Compute

$$\hat{\mathcal{X}}_{T+h,s}^{g,*}(u) = \bar{\mathcal{X}}_s^g(u) + \sum_{k=1}^K \hat{\Gamma}_{k,T+h,s}^{g,*} \hat{\phi}_{k,s}^g(u) + U_{T+h,s}^{g,*}(u),$$

where $U_{T+h,s}^{g,*}(u)$ is iid resampled from the set $\{U_{t,s}^g(u) - \bar{U}_s^g(u), t = 1, 2, \dots, T\}$, $\bar{U}_s^g(u) = T^{-1} \sum_{t=1}^T U_{t,s}^g(u)$ and $U_{t,s}^g(u) = \hat{\mathcal{X}}_{t,s}^g(u) - \sum_{k=1}^K \hat{\Gamma}_{k,t,s}^g \hat{\phi}_{k,s}^g(u)$. In this step, it is assumed that the basis functions $\hat{\phi}_{k,s}^g(u)$ remain fixed during the bootstrapping process, which is conducted using the forward VAR of the principal component scores.

- 4) Fit a VAR(p) process to the “backward” series of the estimated scores; that is,

$$\hat{\Gamma}_{v,s}^g = \sum_{j=1}^p B_{j,p} \hat{\Gamma}_{v+j,s}^g + \zeta_{v,s}^g, \quad v = 1, 2, \dots, T-p,$$

where $B_{j,p}$ denotes the backward VAR(p) coefficient.

5) Generate a pseudo-time series of the scores $\{\widehat{\Gamma}_{1,s}^{g,*}, \dots, \widehat{\Gamma}_{T,s}^{g,*}\}$ by setting $\widehat{\Gamma}_{t,s}^{g,*} = \widehat{\Gamma}_{t,s}^g$ for $t = T, T-1, \dots, T-w+1$, and by using for $t = T-w, T-w-1, \dots, 1$, the backward VAR representation $\widehat{\Gamma}_{v,s}^{g,*} = \sum_{j=1}^p B_{j,p} \widehat{\Gamma}_{v+j,s}^{g,*} + \zeta_{v,s}^{g,*}$.

6) Generate a pseudo-functional time series $\{\widehat{\mathcal{X}}_{1,s}^{g,*}, \dots, \widehat{\mathcal{X}}_{T,s}^{g,*}\}$ as follows. For $t = T, T-1, \dots, T-w+1$ set

$$\widehat{\mathcal{X}}_{t,s}^{g,*}(u) = \overline{\mathcal{X}}_s^g(u) + \sum_{k=1}^K \widehat{\Gamma}_{k,t,s}^g \widehat{\phi}_{k,s}^g(u) + U_{t,s}^g(u),$$

and w is a user-specific tuning parameter, while for $t = T-w, T-w-1, \dots, 1$, use the obtained backward pseudo-scores $\widehat{\Gamma}_{1,s}^{g,*}, \dots, \widehat{\Gamma}_{T-w,s}^{g,*}$ and calculate

$$\widehat{\mathcal{X}}_{t,s}^{g,*}(u) = \overline{\mathcal{X}}_s^g(u) + \sum_{k=1}^K \widehat{\Gamma}_{k,t,s}^{g,*} \widehat{\phi}_{k,s}^g(u) + U_{t,s}^{g,*}(u).$$

where $U_{t,s}^{g,*}(u)$ are iid pseudo-elements. In [Paparoditis and Shang \(2023\)](#), $w = 1$, that is, the bootstrap samples are the same as the most recent curve.

7) For each bootstrapped $\widehat{\mathcal{X}}_{t,s}^{g,*}(u)$, we apply a functional time series forecasting method to obtain its h -step-ahead forecast, denoted by $\widehat{\mathcal{X}}_{T+h|T,s}^{g,*}(u)$.

8) The model calibration error, $\omega_{T+h,s}^{g,*}(u) = \widehat{\mathcal{X}}_{T+h,s}^{g,*}(u) - \widehat{\mathcal{X}}_{T+h|T,s}^{g,*}(u)$, is the difference between the VAR extrapolated forecasts in Step 3) and the model-based forecasts in Step 7).

9) We compute the pointwise standard deviation based on $(\omega_{T+h,s'}^{g,1}, \dots, \omega_{T+h,s}^{g,B})$ where B denotes the total number of bootstrap samples. As in [Aue et al. \(2015\)](#), we search for an optimal tuning parameter δ , where the symmetric prediction interval $(-\delta \times \text{sd}[\omega_{T+h,s'}^{g,1}, \dots, \omega_{T+h,s}^{g,B}], \delta \times \text{sd}[\omega_{T+h,s'}^{g,1}, \dots, \omega_{T+h,s}^{g,B}])$ achieves the smallest coverage probability difference between the empirical and nominal coverage probabilities based on the in-sample data.

10) Using the same functional time-series forecasting method, we apply it to the original functional time series to obtain the h -step-ahead forecast, denoted by $\widehat{\mathcal{X}}_{T+h|T,s}^g(u)$. The symmetric prediction interval can be obtained from Step 9), with the selected δ .

11) We add the deterministic component from the functional ANOVA decomposition used to obtain the functional residuals you started with in step 3.4 to the bootstrap samples obtained in § 3.4. The prediction interval of age-specific mortality curves is

$$\widehat{\mathcal{Y}}_{T+h|T,s}^{g,\ell}(u) = \widehat{\mu}(u) + \widehat{\alpha}_s(u) + \widehat{\beta}^g(u) + \widehat{\mathcal{X}}_{T+h|T,s}^{g,\ell}(u),$$

where ℓ symbolizes either the lower or upper bound.

4 Forecast accuracy evaluation of sub-national mortality data

The forecasting method based on a functional ANOVA decomposition and FPCA is applied to the three datasets, namely the age- and sex-specific mortality rates for the US, France, and Japan. In § 4.1, we explain a forecasting scheme for computing point forecasts and evaluating accuracy using two measures of point forecast error. In § 4.2, we focus on the interval forecasts and the computation of empirical coverage probability. We present the point and interval forecasting results in § 4.1.1 and § 4.2.1 respectively. We evaluate and compare our proposed method based on the estimation of the functional ANOVA model (FMP-ANOVA and FM-ANOVA) with two benchmark functional factor models (Gao et al., 2019; Tavakoli et al., 2023). In the Appendix A.2, we compare the proposed method with a naïve approach by treating each population independently.

4.1 Point forecast evaluation

We consider the rolling window scheme to assess the point forecast as described in Zivot and Wang (2006, Chapter 9). The procedure is carried out as follows:

- 1) The mortality curves are decomposed through a two-way functional ANOVA described in § 3.1 into deterministic and functional residual components. The two factors are the states s and two populations (F and M). The functional residual curves $\widehat{\mathcal{X}}_s^g(u) = [\widehat{\mathcal{X}}_{1,s}^g(u), \dots, \widehat{\mathcal{X}}_{T,s}^g(u)]$ are the ones obtained after removing all deterministic components.
- 2) We start by performing a h -step-ahead point forecast of the functional residual component. Then, we add the deterministic components to obtain the point forecast of the future curves.
- 3) To compute each of the h -step-ahead point forecasts, for $h = 1, \dots, H$, we proceed as follows: for the h -step-ahead point forecast, we consider a rolling window as a training set of size T and produce a $(T + h)$ -step-ahead point forecast, and add back the deterministic components.
- 4) The process iterates over h , and the training set rolls one-step-ahead each time until $T + H$.

We use the relative root mean squared prediction error (RMSPE) and the mean absolute prediction error (MAPE) to evaluate the point forecast accuracy. They measure how close the

forecasts are compared to the actual values of the forecast variable. We compute the relative RMSPE and the relative MAPE for each of the states and genders as

$$\begin{aligned} \text{RMSPE}_s^g(h) &= \sqrt{\frac{1}{Hp} \sum_{\zeta=h}^H \sum_{i=1}^p \left[\frac{\mathcal{Y}_{T+\zeta,s}^g(u_i) - \hat{\mathcal{Y}}_{T+\zeta,s}^g(u_i)}{\mathcal{Y}_{T+\zeta,s}^g(u_i)} \right]^2} \times 100 \\ \text{MAPE}_s^g(h) &= \frac{1}{Hp} \sum_{\zeta=h}^H \sum_{i=1}^p \left| \frac{\mathcal{Y}_{T+\zeta,s}^g(u_i) - \hat{\mathcal{Y}}_{T+\zeta,s}^g(u_i)}{\mathcal{Y}_{T+\zeta,s}^g(u_i)} \right| \times 100, \end{aligned}$$

where $\mathcal{Y}_{T+\zeta,s}^g(u_i)$ represents the holdout sample for state s and gender g . $\hat{\mathcal{Y}}_{T+\zeta,s}^g(u_i)$ represents the corresponding point forecasts.

For the considered disaggregation level by state s and population g , in § 4.1.1, we report the average measurement of point forecasts over the whole forecasting horizon $H = 10$, leading to a mean RMSPE and mean MAPE given by

$$\begin{aligned} \overline{\text{RMSPE}}_s^g &= \frac{1}{H} \sum_{h=1}^H \text{RMSPE}_s^g(h) \\ \overline{\text{MAPE}}_s^g &= \frac{1}{H} \sum_{h=1}^H \text{MAPE}_s^g(h). \end{aligned}$$

4.1.1 Point forecast comparison

We present the results for the point forecasts for the three datasets considered: the US, France, and Japan. Averaging over the $H = 10$ time horizon at each state s and gender g , Figure 2 presents the mean(RMSPE) and mean(MAPE) values using the proposed approaches: FMP-ANOVA (most left), FM-ANOVA (left), the functional factor models from Gao et al. (2019) (right), and Tavakoli et al. (2023) (most right). Figure 2 represents the results for the average obtained by each of the states for the two considered populations, male (in blue) and female (in orange) when forecasting.

We can observe that our proposed approach shows better performance for point forecasting in each of the three datasets. In particular, in the first and third rows of Figure 2, FM-ANOVA shows a much better point forecast result compared to the FMP-ANOVA, though the FMP-ANOVA attains better results compared to the benchmark methods. The most homogeneous behavior in mortality rates for Japan compared to the US and France is not surprising given Japan's low mortality rates in relation to other G7 nations (Tsugane, 2020). In terms of population, we can see that in the cases of the US and France, male forecasting errors are slightly larger than female forecasting errors. The individual forecast errors for horizons $h = 1, \dots, H$, obtained from both methods for each state, are available in a developed shiny app <https://cristianjv.shinyapps.io/HDFTSForecasting/>.

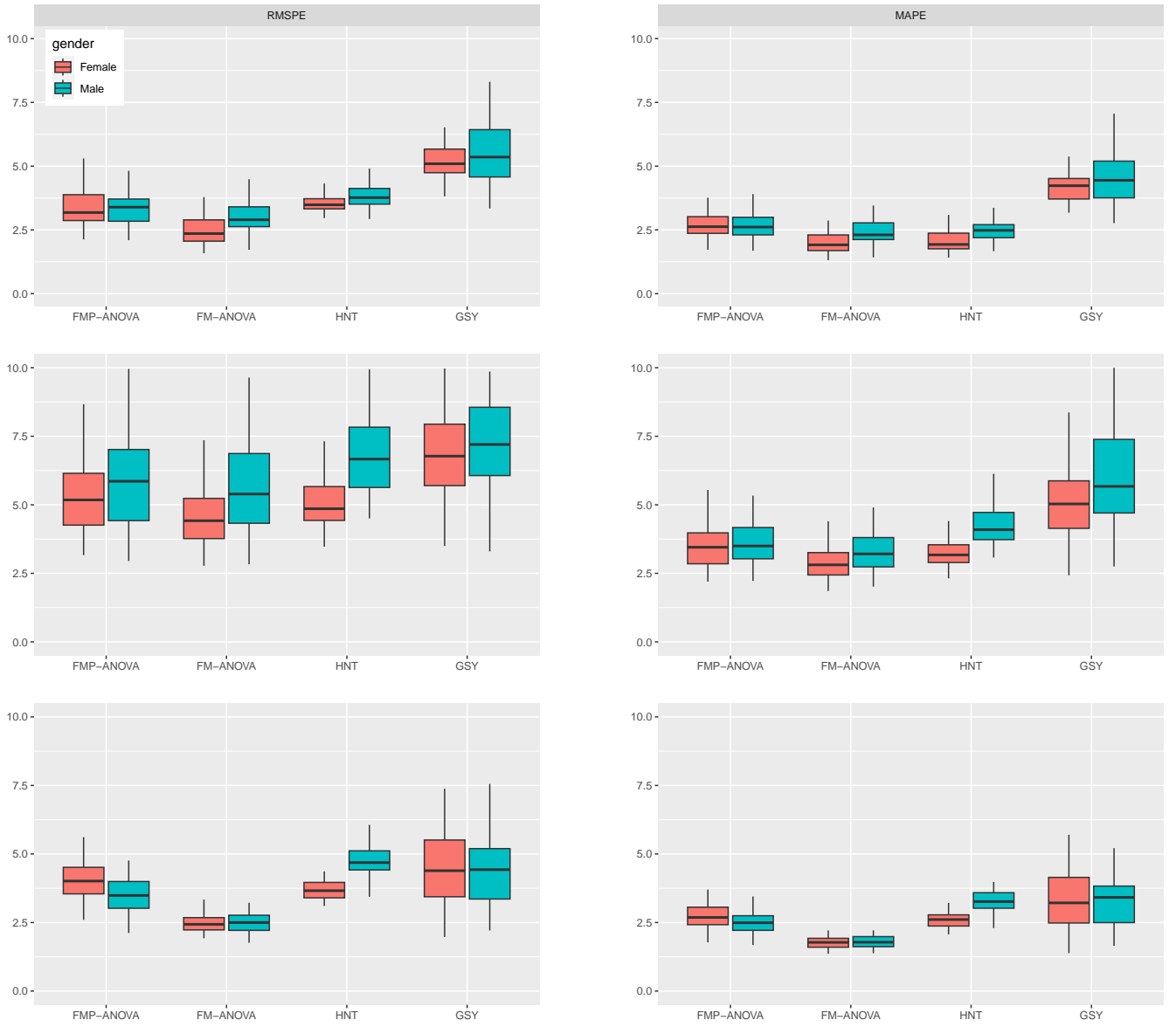


Figure 2: The point forecast error, averaged across states, is calculated based on the estimation of the covariance operator, and the retained components are estimated by the eigenvalue ratio criterion (EVR). The results are presented in three rows: the first row corresponds to the US, the second to France, and the third to Japan. The left column displays the RMSPE, while the right column displays the MAPE. HNT refers to the method of [Tavakoli et al. \(2023\)](#), while GSY refers to the method of [Gao et al. \(2019\)](#).

4.2 Interval forecast evaluation

To evaluate pointwise interval forecast accuracy, we consider the coverage probability difference (CPD) between the nominal and empirical coverage probabilities. The empirical coverage

probability is defined as follows

$$\text{Empirical coverage}_s^g = 1 - \frac{1}{Hp} \sum_{\zeta=h}^H \sum_{i=1}^p \left[\mathbb{1} \left\{ \mathcal{Y}_{T+\zeta|T,s}^g(u_i) > \widehat{\mathcal{Y}}_{T+\zeta|T,s}^{g,\text{ub}}(u_i) \right\} + \mathbb{1} \left\{ \mathcal{Y}_{T+\zeta|T,s}^g(u_i) < \widehat{\mathcal{Y}}_{T+\zeta|T,s}^{g,\text{lb}}(u_i) \right\} \right],$$

where H denotes the number of curves in the forecasting period, p denotes the number of discretized points for the age, $\widehat{\mathcal{Y}}_{T+\zeta|T,s}^{g,\text{ub}}$ and $\widehat{\mathcal{Y}}_{T+\zeta|T,s}^{g,\text{lb}}$ denote the upper and lower bounds of the corresponding forecasted interval, and $\mathbb{1}\{\cdot\}$ the binary indicator function. Pointwise CPD is defined as

$$\text{CPD}_s^g = \left| \text{Empirical coverage}_s^g - \text{Nominal coverage} \right|.$$

The lower the CPD_s^g value, the better the forecasting method's performance.

Additionally, we utilize the interval score of [Gneiting and Raftery \(2007\)](#) (see also [Gneiting and Katzfuss, 2014](#)). For each year in the forecasting period, the h -step-ahead prediction intervals were calculated at the $100(1 - \alpha)\%$ nominal coverage probability. We consider the common case of the symmetric $100(1 - \alpha)\%$ prediction interval, with lower and upper bounds that are predictive quantiles at $\alpha/2$ and $1 - \alpha/2$, denoted by $\widehat{\mathcal{Y}}_{T+\zeta|T,s}^{g,\text{lb}}(u_i)$ and $\widehat{\mathcal{Y}}_{T+\zeta|T,s}^{g,\text{ub}}(u_i)$. The scoring rule for the interval forecast at discretized point u_i is

$$\begin{aligned} S_{\alpha,\zeta,s}^g \left[\widehat{\mathcal{Y}}_{T+\zeta|T,s}^{g,\text{lb}}(u_i), \widehat{\mathcal{Y}}_{T+\zeta|T,s}^{g,\text{ub}}(u_i), \mathcal{Y}_{T+\zeta|T,s}^g(u_i) \right] &= \left[\widehat{\mathcal{Y}}_{T+\zeta|T,s}^{g,\text{ub}}(u_i) - \widehat{\mathcal{Y}}_{T+\zeta|T,s}^{g,\text{lb}}(u_i) \right] \\ &+ \frac{2}{\alpha} \left[\widehat{\mathcal{Y}}_{T+\zeta|T,s}^{g,\text{lb}}(u_i) - \mathcal{Y}_{T+\zeta|T,s}^g(u_i) \right] \mathbb{1} \left\{ \mathcal{Y}_{T+\zeta|T,s}^g(u_i) < \widehat{\mathcal{Y}}_{T+\zeta|T,s}^{g,\text{lb}}(u_i) \right\} \\ &+ \frac{2}{\alpha} \left[\mathcal{Y}_{T+\zeta|T,s}^g(u_i) - \widehat{\mathcal{Y}}_{T+\zeta|T,s}^{g,\text{ub}}(u_i) \right] \mathbb{1} \left\{ \widehat{\mathcal{Y}}_{T+\zeta|T,s}^{g,\text{ub}}(u_i) > \mathcal{Y}_{T+\zeta|T,s}^g(u_i) \right\}, \end{aligned}$$

where $\mathbb{1}\{\cdot\}$ represents the binary indicator function, and α denotes a level of significance. Finally, we compute the mean interval score for the total of T series as

$$\bar{S}_{\alpha,s}^g = \frac{1}{Hp} \sum_{\zeta=h}^H \sum_{i=1}^p S_{\alpha,\zeta,s}^g \left[\widehat{\mathcal{Y}}_{T+\zeta|T,s}^{g,\text{lb}}(u_i), \widehat{\mathcal{Y}}_{T+\zeta|T,s}^{g,\text{ub}}(u_i), \mathcal{Y}_{T+\zeta|T,s}^g(u_i) \right].$$

The optimal interval score is achieved when $\mathcal{Y}_{T+\zeta|T,s}^g(u_i)$ lies between $\widehat{\mathcal{Y}}_{T+\zeta|T,s}^{g,\text{lb}}(u_i)$ and $\widehat{\mathcal{Y}}_{T+\zeta|T,s}^{g,\text{ub}}(u_i)$, with the distance between the upper bound and the lower bound being minimal.

4.2.1 Interval forecast comparison

We present the interval forecast results for the three datasets: the US, France, and Japan. Interval forecasts are assessed when constructed using both the proposed FMP-ANOVA (Figure 3) and

FM-ANOVA (Figure 4) approaches. The averages correspond to each of the states for all data examples. We present the averages across the forecasting horizon of $H = 10$ years ahead for two different interval forecasting accuracies: empirical coverage probability (top panel), coverage probability difference (CPD) (middle panel); and mean interval score (bottom panel).

In the first row of Figures 3 and 4, we present the pointwise coverage probability for both male and female populations. For each of the countries, we consider two nominal coverages: 80% and 95%. For the FMP-ANOVA approach in Figure 3, by examining the median level of the averages for the pointwise coverage probability, we can see that all three nations and both populations are very close to the nominal levels. However, the FMP-ANOVA approach performs better for the French dataset towards the 95% nominal level than the 80% nominal level for both males and females. The FMP-ANOVA approach outperforms the case of the US compared to the other two countries in population and nominal levels. The Japanese dataset achieves a level similar to the 80%, although the median level in the 95% example seems to be lower.

In contrast, when using the FM-ANOVA in Figure 4, we can observe that for France, the 80% nominal level at the median level of the empirical coverage probability is upper skewed, while for the other two countries, it remains very similar to the nominal level, performing better. Similar to the results from the FMP-ANOVA, we can observe that the forecast intervals with the 95% nominal level perform much better.

In the same line as with the pointwise coverage probability, and to make the interpretation of the results easier, in the second row of Figures 3 and 4, we present the CPD for both populations as well as both nominal levels. In general, we can observe that for the three countries, the 95% nominal level achieves the lowest range of values of the CPD. Regarding the 80% nominal level, the FMP-ANOVA produced superior results in the case of the US over the case of France. In contrast, in the case of Japan, both approaches outperformed France. In Figure 4 with the 95% nominal level, FM-ANOVA yields the narrowest range of values for the cases of the US and France, which outperform the Japanese case in terms of CPD. The third row of Figures 3 and 4 presents the results for the mean interval score for both populations. In general, according to both methodologies, the interval score shows better performance in the case of France than in the other two countries; nonetheless, the case of the US has the best overall average interval score performance.

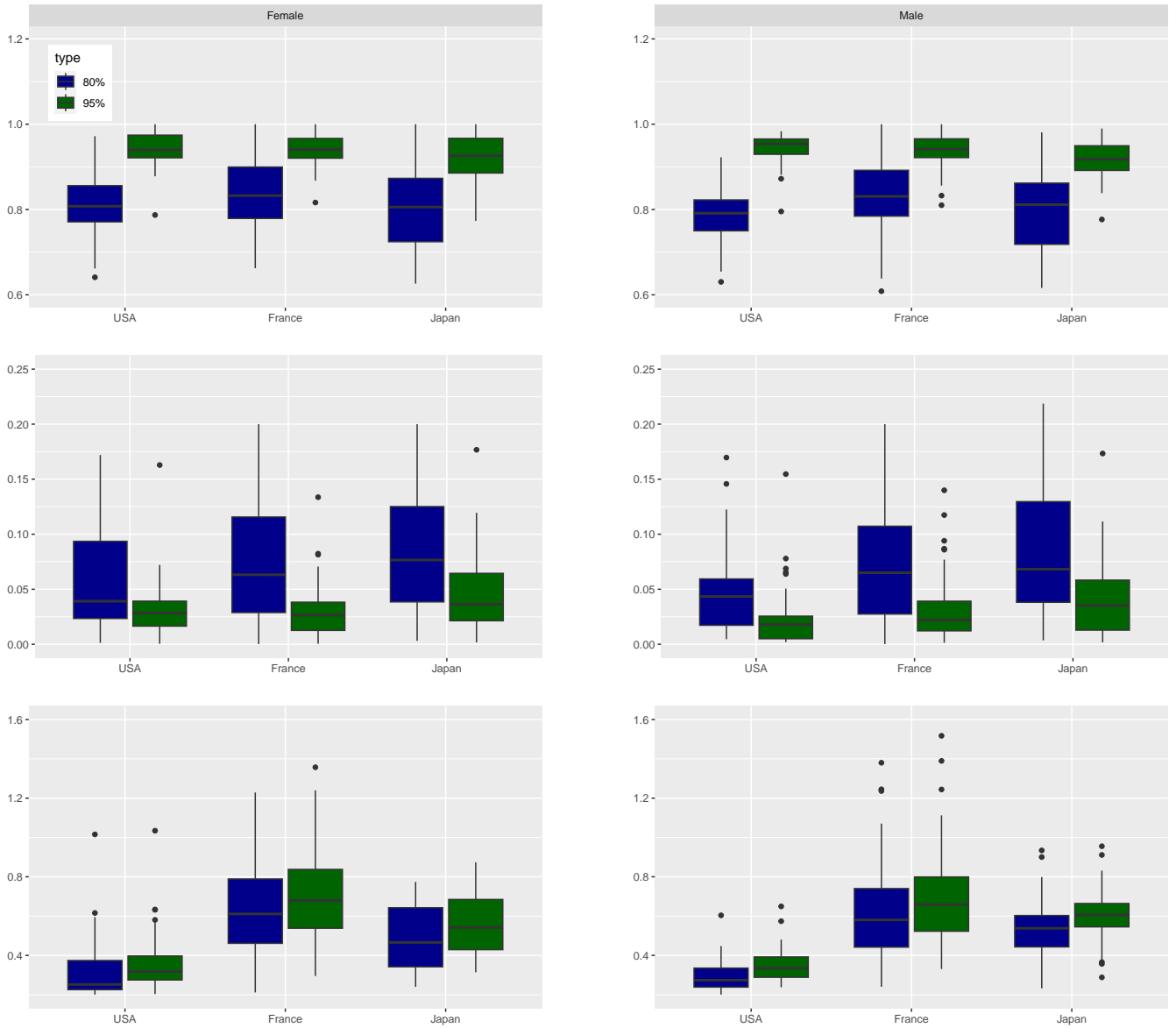


Figure 3: The plot displays the results of interval prediction performance across states for all three countries using the FMP-ANOVA decomposition. The top row represents the pointwise empirical coverage probability. The middle row shows the coverage probability difference (CPD). The bottom row presents the mean interval score. The left panel corresponds to the female population, while the right panel corresponds to the male population. Two nominal coverage probabilities are considered: 80% and 95%. Each plot includes data for the United States (leftmost), France (center), and Japan (rightmost).

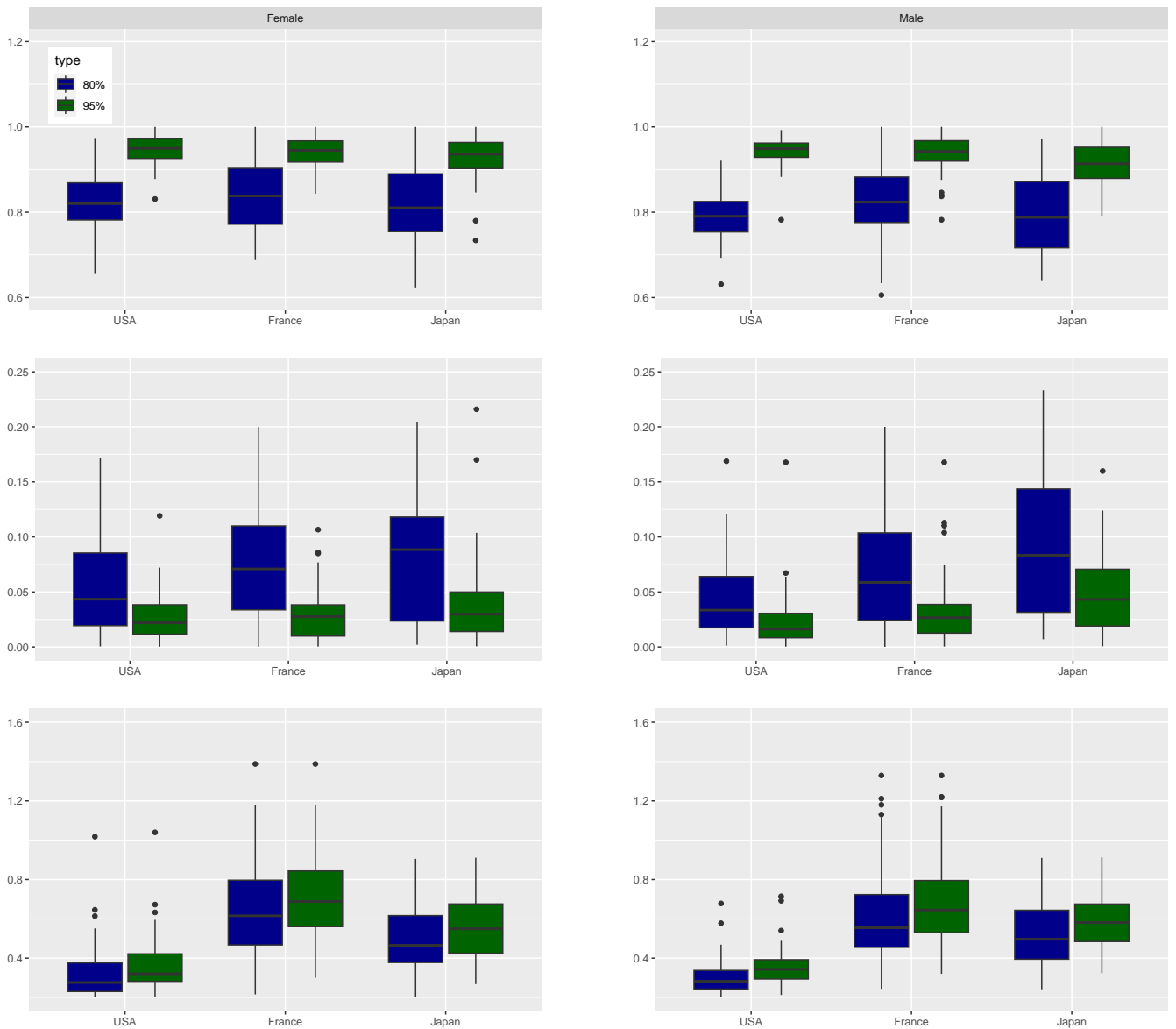


Figure 4: The plot displays the results of interval prediction performance across states for all three countries using the FM-ANOVA decomposition. The top row represents the pointwise empirical coverage probability. The middle row shows the coverage probability difference (CPD). The bottom row presents the mean interval score. The left panel corresponds to the female population, while the right panel corresponds to the male population. Two nominal coverage probabilities are considered: 80% and 95%. Each plot includes data for the United States (leftmost), France (center), and Japan (rightmost).

5 Conclusion

We have proposed an innovative FTS forecasting methodology based on the two-way functional median polish. The proposed strategy is useful for FTS models with complex structures, particularly those involving states and various populations. This method of forecasting grouped FTS is derived by combining an estimated two-way functional ANOVA model with the FPCA framework. Using age-specific mortality rates at the national and sub-national levels in the US, France, and Japan, we compare the averages across the 10 point forecast accuracies for the proposed method based on functional-ANOVA decomposition with several benchmark methods like the factor models of [Gao et al. \(2019\)](#) and [Tavakoli et al. \(2023\)](#) and independent FTS (see Appendix A.2). We can see that the two-way functional ANOVA decomposition strategy beats benchmark methods.

There are several ways in which the present methodology can be further extended, and we briefly mention four.

1) First, one restriction of the proposed method is the possibility of outliers, which may significantly impact the modeling and forecasting of principal component scores. Using a robust functional principal component approach (see, e.g., [Bali et al., 2011](#)) or other robust time series methods (see, e.g., [Gelper et al., 2010](#)) are possible approaches for addressing this issue.

2) Second, other levels of disaggregation may be included in the suggested approach with the availability of appropriate data. Cause-of-death, as mentioned in [Arnold and Sherris \(2015\)](#) and socioeconomic status ([Singh et al., 2013](#)) are examples of such levels. In the same spirit, we may incorporate different mortality data measures, such as the age distribution of death counts as in [Shang and Haberman \(2020\)](#) and [Shang et al. \(2022\)](#).

3) Third, the proposed methodology may be employed in other application areas, such as university performance completion rates, which can be disaggregated by age, gender, faculty, local or international status, and other criteria. Such disaggregation levels enable us to employ joint forecast approaches that use constrained estimates of age-specific completion rates to quantify the effect of various factors that may explain completion behavior.

4) The functional residual component, which exhibits time-varying characteristics and is derived from estimating the two-way functional ANOVA model, can be regarded as a functional time series (FTS) on its own. Consequently, employing functional factor models, such as the one proposed by [Tavakoli et al. \(2023\)](#), is a viable approach to enhance the forecasting accuracy of this component.

Supplementary Materials

Code for FTS forecasting based on FMP-ANOVA and FM-ANOVA. The R code to produce point and interval forecasts from the two approaches described in the paper. The R codes are available at the following repository: https://github.com/cfjimenezv07/Forecasting_HDFTS/tree/main/Rcodes_paper

Code for shiny application. The R code to produce a shiny user interface for plotting every series and the results for point and interval forecasts for the three considered mortality databases. The R codes are available at the following repository: https://github.com/cfjimenezv07/Forecasting_HDFTS/tree/main/Shiny_app

Acknowledgement

The first author acknowledges the financial support of the King Abdullah University of Science and Technology (KAUST). The last author acknowledges the funding of an Australian Research Council Discovery Project DP230102250 titled “Feature learning for high-dimensional functional time series” and Macquarie University DataX consilience center. The authors are grateful for the comments from the participants at the Australian National University, University of Auckland, Australian Government Actuary, the 6th International Conference on Econometrics and Statistics (EcoSta 2023), Joint Statistical Meeting, and Australian Statistical Conference in 2023.

References

- Ahn, S. C. and A. R. Horenstein (2013). Eigenvalue ratio test for the number of factors. *Econometrica* 81(3), 1203–1227.
- Antoniadis, A., X. Brossat, J. Cugliari, and J.-M. Poggi (2016). A prediction interval for a function-valued forecast model: Application to load forecasting. *International Journal of Forecasting* 32(3), 939–947.
- Antoniadis, A., E. Paparoditis, and T. Sapatinas (2006). A functional wavelet–kernel approach for time series prediction. *Journal of the Royal Statistical Society Series B* 68(5), 837–857.

- Arnold, S. -G. and M. Sherris (2015). Causes-of-death mortality: What do we know on their dependence? *North American Actuarial Journal* 19(2), 116–128.
- Aue, A., D. D. Norinho, and S. Hörmann (2015). On the prediction of stationary functional time series. *Journal of the American Statistical Association: Theory and Methods* 110, 378–392.
- Bali, J. L., G. Boente, D. E. Tyler, and J.-L. Wang (2011). Robust functional principal components: A projection-pursuit approach. *The Annals of Statistics* 39(6), 2852 – 2882.
- Basellini, U. and C. G. Camarda (2019). Modelling and forecasting adult age-at-death distributions. *Population Studies* 73(1), 119–138.
- Basellini, U., C. G. Camarda, and H. Booth (2023). Thirty years on: A review of the Lee–Carter method for forecasting mortality. *International Journal of Forecasting* 39(3), 1033–1049.
- Bonnet, F. (2020). Computations of French lifetables by departments, 1901-2014. *Demographic Research* 42, 741–762.
- Booth, H. (2006). Demographic forecasting: 1980 to 2005 in review. *International Journal of Forecasting* 22(3), 547–581.
- Booth, H. and L. Tickle (2008). Mortality modelling and forecasting: a review of methods. *Annals of Actuarial Science* 3(1-2), 3–43.
- Brumback, B. A. and J. A. Rice (1998). Smoothing spline models for the analysis of nested and crossed samples of curves. *Journal of the American Statistical Association: Theory and Methods* 93(443), 961–976.
- Chang, J., C. Chen, X. Qiao, and Q. Yao (2023). An autocovariance-based learning framework for high-dimensional functional time series. *Journal of Econometrics in press*.
- Chiou, J.-M. (2012). Dynamical functional prediction and classification with application to traffic flow prediction. *The Annals of Applied Statistics* 6(4), 1588–1614.
- Currie, I. D., M. Durban, and P. H. Eilers (2004). Smoothing and forecasting mortality rates. *Statistical Modelling* 4(4), 279–298.

- Emerson, J. D. and D. C. Hoaglin (1983). Analysis of two-way tables by medians. In D. C. Hoaglin, F. Mosteller, and J. W. Tukey (Eds.), *Understanding Robust and Exploratory Data Analysis*, pp. 166–210. New York: Wiley.
- Gao, Y., H. L. Shang, and Y. Yang (2019). High-dimensional functional time series forecasting: An application to age-specific mortality rates. *Journal of Multivariate Analysis* 170, 232–243.
- Gelper, S., R. Fried, and C. Croux (2010). Robust forecasting with exponential and holt–winters smoothing. *Journal of Forecasting* 29(3), 285–300.
- Giroi, F. and G. King (2008). *Demographic Forecasting*. Princeton: Princeton University Press.
- Gneiting, T. and M. Katzfuss (2014). Probabilistic forecasting. *The Annual Review of Statistics and Its Application* 1, 125–151.
- Gneiting, T. and A. E. Raftery (2007). Strictly proper scoring rules, prediction, and estimation. *Journal of the American Statistical Association: Review Article* 102(477), 359–378.
- Guo, S. and X. Qiao (2023). On consistency and sparsity for high-dimensional functional time series with application to autoregressions. *Bernoulli* 29(1), 451–472.
- Guo, S., X. Qiao, and Q. Wang (2022). Factor modelling for high-dimensional functional time series. Technical report, arXiv. <https://arxiv.org/abs/2112.13651>.
- Hall, P. and M. Hosseini-Nasab (2006). On properties of functional principal components analysis. *Journal of the Royal Statistical Society: Series B (Statistical Methodology)* 68(1), 109–126.
- Hall, P., H.-G. Müller, and J.-L. Wang (2006). Properties of principal component methods for functional and longitudinal data analysis. *The Annals of Statistics* 34(3), 1493 – 1517.
- Hall, P. and C. Vial (2006). Assessing the finite dimensionality of functional data. *Journal of the Royal Statistical Society: Series B* 68(4), 689–705.
- Hallin, M., G. Nisol, and S. Tavakoli (2023). Factor models for high-dimensional functional time series i: Representation results. *Journal of Time Series Analysis* 44(5-6), 578–600.
- Hyndman, R. and M. S. Ullah (2007). Robust forecasting of mortality and fertility rates: A functional data approach. *Computational Statistics and Data Analysis* 51(10), 4942–4956.

- Hyndman, R. J., H. Booth, and F. Yasmeen (2013a). Coherent mortality forecasting: the product-ratio method with functional time series models. *Demography* 50(1), 261–283.
- Hyndman, R. J., H. Booth, and F. Yasmeen (2013b, February). Coherent mortality forecasting: the product-ratio method with functional time series models. *Demography* 50(1), 261–283.
- Hyndman, R. J. and H. L. Shang (2009). Forecasting functional time series. *Journal of the Korean Statistical Society* 38(3), 199–211.
- Japanese Mortality Database (2023). *National Institute of Population and Social Security Research*. National Institute of Population and Social Security Research. Available at <https://www.ipss.go.jp/p-toukei/JMD/index-en.asp> (data downloaded on March 15, 2023).
- Kaufman, C. G. and S. R. Sain (2010). Bayesian functional ANOVA modeling using Gaussian process prior distributions. *Bayesian Analysis* 5(1), 123 – 149.
- Lam, C. and Q. Yao (2012). Factor modeling for high-dimensional time series: Inference for the number of factors. *The Annals of Statistics* 40, 694–726.
- Lee, R. D. and L. R. Carter (1992). Modeling and forecasting U.S. mortality. *Journal of the American Statistical Association: Applications & Case Studies* 87(419), 659–671.
- Li, D., R. Li, and H. L. Shang (2023). Detection and estimation of structural breaks in high-dimensional functional time series. Technical report, arXiv.
- Li, D., P. M. Robinson, and H. L. Shang (2021). Local Whittle estimation of long-range dependence for functional time series. *Journal of Time Series Analysis* 42(5-6), 685–695.
- Li, J. (2012). A Poisson common factor model for projecting mortality and life expectancy jointly for females and males. *Population Studies* 67(1), 111–126.
- Li, N., R. Lee, and P. Gerland (2013). Extending the Lee-Carter method to model the rotation of age patterns of mortality decline for long-term projections. *Demography* 50(6), 2037–2051.
- Locantore, N., J. S. Marron, D. G. Simpson, N. Tripoli, J. T. Zhang, K. L. Cohen, G. Boente, R. Fraiman, B. Brumback, C. Croux, J. Fan, A. Kneip, J. I. Marden, D. Peña, J. Prieto, J. O. Ramsay, M. J. Valderrama, A. M. Aguilera, N. Locantore, J. S. Marron, D. G. Simpson, N. Tripoli,

- J. T. Zhang, and K. L. Cohen (1999). Robust principal component analysis for functional data. *Test* 8(1), 1–73.
- Mercer, J. and A. R. Forsyth (1909). Xvi. functions of positive and negative type, and their connection the theory of integral equations. *Philosophical Transactions of the Royal Society of London. Series A, Containing Papers of a Mathematical or Physical Character* 209(441-458), 415–446.
- Mosteller, F. and J. W. Tukey (1977). *Data Analysis and Regression*. Cambridge: Addison-Wesley.
- Pampel, F. (2005). Forecasting sex differences in mortality in high income nations: the contribution of smoking. *Demographic Research* 13(18), 455–484.
- Paparoditis, E. (2018). Sieve bootstrap for functional time series. *The Annals of Statistics* 46, 3510–3538.
- Paparoditis, E. and H. L. Shang (2023). Bootstrap prediction bands for functional time series. *Journal of the American Statistical Association: Theory and Methods* 118(542), 972–986.
- Ramsay, J. and B. Silverman (2006). *Functional Data Analysis*. Springer Series in Statistics. New York: Springer.
- Raña, P., G. Aneiros, J. Vilar, and P. Vieu (2016). Bootstrap confidence intervals in functional nonparametric regression under dependence. *Electronic Journal of Statistics* 10(2), 1973 – 1999.
- Renshaw, A. E. and S. Haberman (2003). Lee-Carter mortality forecasting with age-specific enhancement. *Insurance: Mathematics and Economics* 33(2), 255–272.
- Shang, H. L. (2014). A survey of functional principal component analysis. *AStA Advances in Statistical Analysis* 98, 121–142.
- Shang, H. L. (2016). Mortality and life expectancy forecasting for a group of populations in developed countries: A multilevel functional data method. *The Annals of Applied Statistics* 10, 1639–1672.
- Shang, H. L., H. Booth, and R. J. Hyndman (2011). Point and interval forecasts of mortality rates and life expectancy: A comparison of ten principal component methods. *Demographic Research* 25, 173–214.

- Shang, H. L. and S. Haberman (2017). Grouped multivariate and functional time series forecasting: An application to annuity pricing. *Insurance: Mathematics and Economics* 75, 166–179.
- Shang, H. L. and S. Haberman (2020). Forecasting age distribution of death counts: An application to annuity pricing. *Annals of Actuarial Science* 14, 150–169.
- Shang, H. L., S. Haberman, and R. Xu (2022). Multi-population modelling and forecasting life-table death counts. *Insurance: Mathematics and Economics* 106, 239–253.
- Shang, H. L. and R. J. Hyndman (2017). Grouped functional time series forecasting: An application to age-specific mortality rates. *Journal of Computational and Graphical Statistics* 26, 330–343.
- Shang, H. L. and Y. Yang (2021). Forecasting Australian subnational age-specific mortality rates. *Journal of Population Research* 38(1), 1–24.
- Singh, G. K., R. E. Azuine, M. Siahpush, and M. D. Kogan (2013). All-cause and cause-specific mortality among US youth: Socioeconomic and rural-urban disparities and international patterns. *Journal of Urban Health* 90(3), 388–405.
- Spitzner, D. J., J. S. Marron, and G. K. Essick (2003). Mixed-model functional ANOVA for studying human tactile perception. *Journal of the American Statistical Association: Applications & Case Studies* 98(462), 263–272.
- Sun, Y. and M. G. Genton (2012). Functional median polish. *Journal of Agricultural, Biological, and Environmental Statistics* 17(3), 354–376.
- Tan, J., D. Liang, Y. Guan, and H. Huang (2024). Graphical principal component analysis of multivariate functional time series. *Journal of the American Statistical Association: Theory and Methods* in press.
- Tang, C., H. L. Shang, and Y. Yang (2022). Clustering and forecasting multiple functional time series. *The Annals of Applied Statistics* 16(4), 2523–2553.
- Tavakoli, S., G. Nisol, and M. Hallin (2023). Factor models for high-dimensional functional time series ii: Estimation and forecasting. *Journal of Time Series Analysis* 44(5-6), 601–621.
- Tsugane, S. (2020). Why has japan become the world’s most long-lived country: Insights from a food and nutrition perspective.

- Tukey, J. (1977). *Exploratory Data Analysis*. Reading: Addison-Wesley.
- United States Mortality Database (2023). *University of California, Berkeley (USA)*. Department of Demography at the University of California, Berkeley. Available at usa.mortality.org (data downloaded on March 15, 2023).
- Vilar, J., G. Aneiros, and P. Raña (2018). Prediction intervals for electricity demand and price using functional data. *International Journal of Electrical Power & Energy Systems* 96, 457–472.
- Viviani, R., G. Grön, and M. Spitzer (2005). Functional principal component analysis of fMRI data. *Human Brain Mapping* 24(2), 109–129.
- Wang, J.-L., J.-M. Chiou, and H.-G. Müller (2016). Review of functional data analysis. *Annual Review of Statistics and Its Application* 3, 257–295.
- Wang, Y., C. Ke, and M. B. Brown (2003). Shape-invariant modeling of circadian rhythms with random effects and smoothing spline ANOVA decompositions. *Biometrics* 59(4), 804–812.
- Wiśniowski, A., P. W. F. Smith, J. Bijak, J. Raymer, and J. J. Forster (2015). Bayesian population forecasting: Extending the Lee-Carter method. *Demography* 52(3), 1035–1059.
- Wood, S. N. (1994). Monotonic smoothing splines fitted by cross validation. *SIAM Journal on Scientific Computing* 15(5), 1126–1133.
- Yang, Y., H. L. Shang, and J. Raymer (2024). Forecasting Australian fertility by age, region, and birthplace. *International Journal of Forecasting in press*.
- Yao, F., H.-G. Müller, and J.-L. Wang (2005). Functional data analysis for sparse longitudinal data. *Journal of the American Statistical Association: Theory and Methods* 100(470), 577–590.
- Zhou, Z. and H. Dette (2023). Statistical inference for high-dimensional panel functional time series. *Journal of the Royal Statistical Society: Series B* 85(2), 523–549.
- Zivot, E. and J. Wang (2006). *Modeling Financial Time Series with S-PLUS*. New York: Springer.

A Appendix

A.1 Multivariate time series forecasting approach.

We conducted an additional analysis by fixing the number of retained components at $K = 6$, as it has been shown that this number of components is enough (Hyndman et al., 2013b). In this scenario, we explored the application of a multivariate time series forecasting method, specifically VAR, to conduct the forecasting. To facilitate comparison, Figure 5 presents a comparison between the univariate ARIMA and multivariate VAR time series forecasting methods. Notably, the results from the univariate time series method (ARIMA) demonstrate notably superior forecasting performance.

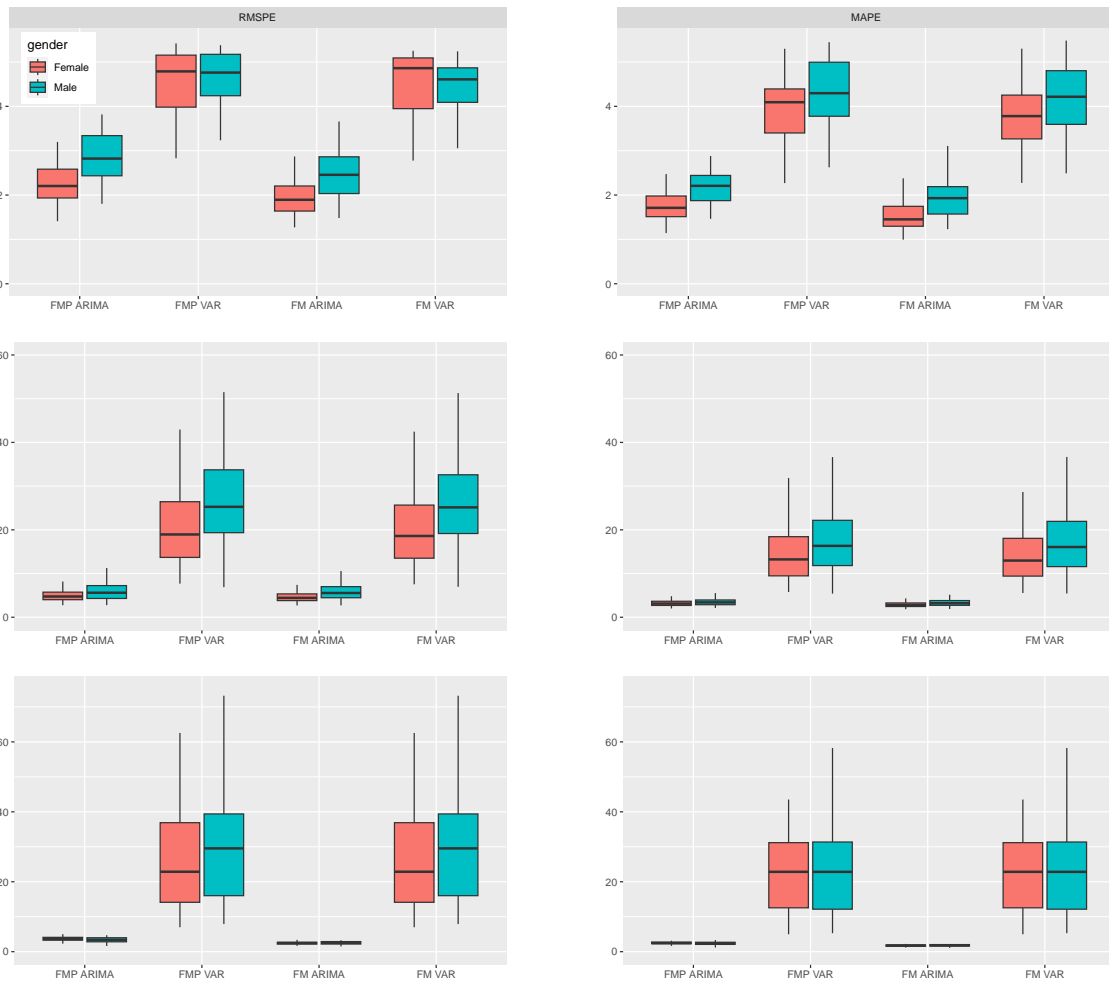


Figure 5: Comparison between the univariate ARIMA and multivariate VAR time series forecasting methods when $K = 6$. The results are presented in three rows: the first row corresponds to the US, the second row to France, and the third row to Japan. The left column displays the relative RMSPE, while the right column displays the relative MAPE.

A.2 Independent populations

In order to establish a real enhancement of the forecasting approach based on the estimation of a two-way functional ANOVA model, in this Appendix, we present the point forecast results of the two proposed estimating methods: FMP-ANOVA and FM-ANOVA in comparison to a naive approach in which all populations are considered to be independent. In Figure 6, we can observe the point forecast errors are larger for all states in the three datasets for the independent forecasting method.

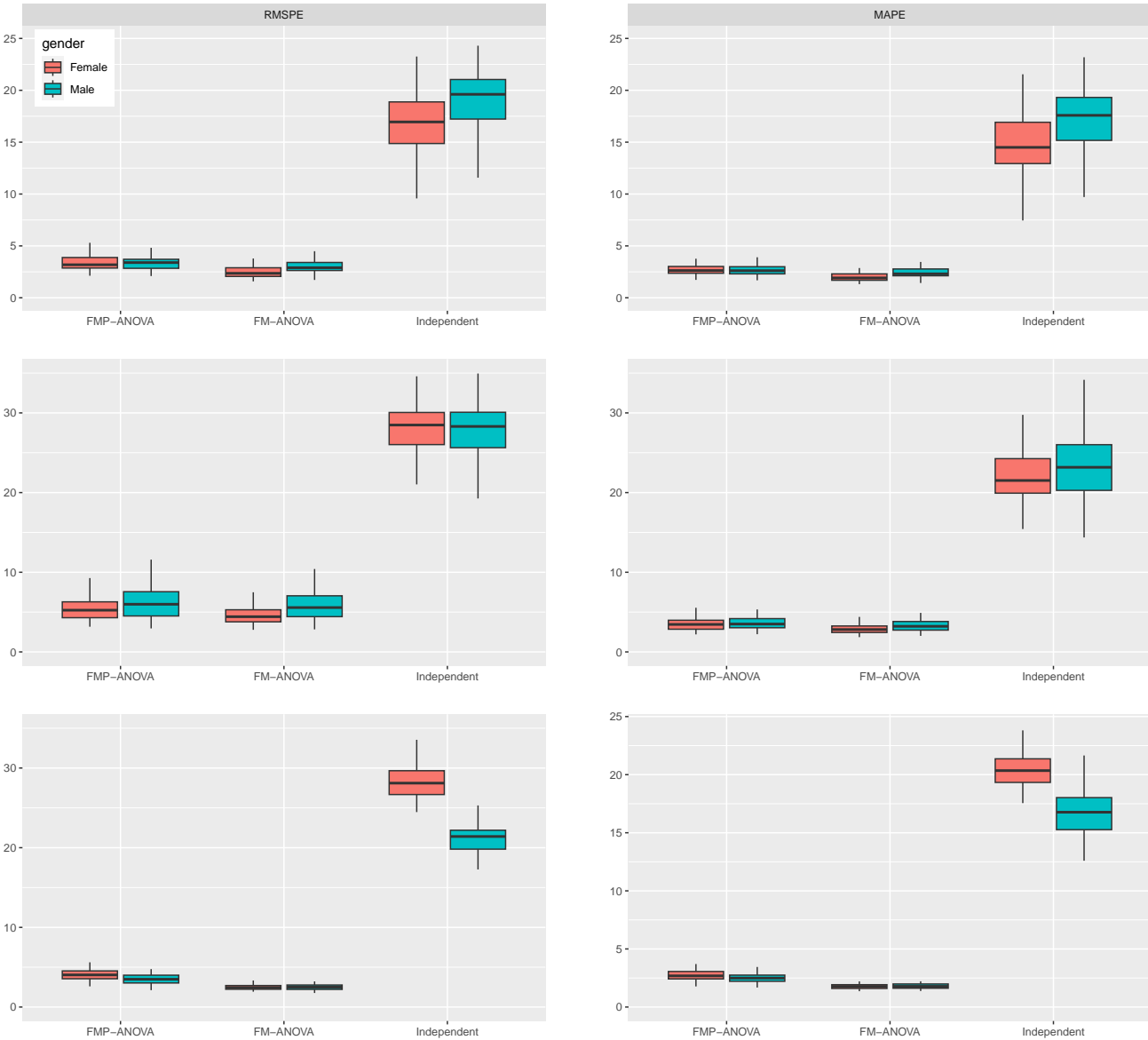


Figure 6: The US average forecast error per state, the French average forecast error per department, and the Japanese average forecast error per prefecture. The relative RMSPE is shown to the left, while the relative MAPE is to the right.